MULTIPHYSICS SIMULATION OF THEMRAL AND FLUID DYNAMICS PHENOMENA DURING THE PULSED LASER POWDER BED FUSION PROCESS OF 316-L STEEL

M. Bayat*, V. K. Nadimpalli, J. H. Hattel

[1]Department of Mechanical Engineering, Technical University of Denmark (DTU), Produktionstorvet 425, Kgs. 2800, Lyngby, Denmark

ABSTRACT

Laser Powder Bed Fusion (L-PBF) has attracted a lot of attention from various industrial sectors and mainly thanks to its well-proven well-known capacity of realizing complex topology-optimized components that have so far been impossible to make using conventional manufacturing techniques. In Pulsed L-PBF (PL-PBF), the laser's temporal profile can be modulated via modifying either or both the cycle duration and the duty cycle. Thus, the laser's temporal profile could be considered as a new process parameter that paves the way for a better control of this process for future applications. Therefore, in this work we aim to investigate how changing the laser's temporal profile can affect the melt pool conditions and the final shape and geometry of a track in the PL-PBF process. In this respect, in this paper a multiphysics numerical model of the PL-PBF process of 316-L stainless steel is developed based on the computational fluid dynamics (CFD) software package Flow-3D and the model is used to simulate the heat and fluid flow conditions occurring inside the melt pool during the course of the process at different pulsing modes. Thus, a parametric study is carried out to study the influence of the laser's cycle duration with a fixed laser duty cycle (50 %) on the shape and size of the melt pool and the final track morphology. It is noticed that at longer cycle periods, more noticeable humps form at the wake of the melt pool as more material is displaced within bigger melt pools, which are at the same time subjected to more significant recoil pressures. It is also observed in the simulations that at 50 % duty cycle, longer melt pools form at 400 μs cycle period compared to the more symmetrical melt pools formed at 1000 μs, primarily because of shorter laser off-times in the former, even though melt pool volume is bigger for the 1000 μs case. The parameteric study illustrates the boundary between a continuous track and a broken track PL-PBF wherein the continuous track is retained by always maintaining a small volume of molten material.

1. INTRODUCTION

L-PBF is a branch of metal additive manufacturing processes that is used to manufacture complex metallic components in a layer-wise manner. In the L-PBF process, a green or red laser irradiates powder particles laying on the powder bed. The amount of delivered energy from the laser is sufficient for melting and even evaporating metallic powder particles. After the solidification of the scanned areas of the powder bed, a consolidated solid part is manufactured and then the base plate moves a small increment along the vertical direction downwards, where the coater adds another layer of powder and then the whole cycle repeats until the entire part is manufactured [1]. The L-PBF process has very well shown its capability to manufacture very exotic and sophisticated geometries designed by topology optimization [2] which have so far been impossible to make using conventional production methods. On the other hand and looking from a physical perspective, L-PBF is a very complex process as there are a wide range of different interdependent physical phenomena occurring while the process runs.

One way of understanding the physics behind the process is via online monitoring methods. These techniques, however, ask for a long preparation time and sometimes also require very expensive equipment such as X-ray beams. Numerical simulations are on the other hand a much cheaper tool used for understanding the physical phenomena during L-PBF. Numerical simulations of L-PBF are divided

*Corresponding Author: mbayat@mek.dtu.dk

into several branches, depending on the type of the involved physics, type of coupling, length-scale and the level of fidelity [3].

As an example, Foroozmehr et al. [4] developed a finite element (FEM) conduction heat transfer model to simulate the temperature evolution around the laser during the L-PBF process of 316-L stainless steel. Lee and Zhang [5] developed an advanced multiphysics model based on the finite volume method (FVM) that accounted for capillary forces and also captured the metal's surface movement. Khairallah et al. [6] developed a multiphysics CFD simulation of the L-PBF of 316-L stainless steel, based on arbitrary Eulerian Lagrangian FEM code. The author group have also developed a series of high-fidelity numerical simulations for modelling different defect formation mechanisms during L-PBF [7,8]. In the past couple of years, there has been a growing interest in melt pool manipulation and controlling techniques via external agents. For instance, Bayat et al. [9] showed how increase in the concentrations of sulfur, as a surface active element, can lead to cooler and at the same time narrower melt pools in L-PBF. Some researchers focused on laser pulsation as a tool to manipulate the melt pool, for example Roehling et al. [10] has recently developed a multiphyiscs model to simulate the thermo-fluid conditions of large area pulsed L-PBF of 316-L stainless steel. Zheng et al. [11] also developed a CFD model based on the Lattice Boltzmann method to simulate the melt pool conditions during point-wise pulsed L-PBF of IN 625.

To the best knowledge of the authors, there is no scientific work on simulating the modulated PL-PBF process where the temporal profile of the laser is changed via modifying the cycle period as well as duty cycle. Therefore in this work we have developed a multiphysics FVM-based CFD model of the modulated PL-PBF process of stainless steel 316-L to investigate how different cycle periods as well as duty cycles can change the melt pool conditions. In the second section, we go through the modelling details as well as the boundary conditions and then we give a brief introduction on how the pulse modulation functions. Then in the third section, we go through results and discussion where we carry out a parametric study with varying cycle durations to understand how these this parameter changes the melt pool temperature and volume as well as the final resultant track shape.

2. MODEL DETAILS AND LASER PULSING

The CFD calculations in this work are carried out in the commercial software package Flow-3D. The incompressible Navier-Stokes equations are solved to find the coupled velocity-pressure fields.

$$\boldsymbol{\nabla} \cdot \mathbf{u} = 0, \tag{1}$$

$$\rho\left[\frac{\partial}{\partial t} + \mathbf{u} \cdot \boldsymbol{\nabla}\right] u = -\boldsymbol{\nabla} p + \mu \nabla^2 \mathbf{u} - \frac{K_c (1-f)^3}{C_k + f^2}\mathbf{u} + \mathbf{F'''}_{\mathbf{interface}}, \tag{2}$$

$$\mathbf{F''}_{\mathbf{interface}} = \left[A_p exp\left[B_p\left(1 - \frac{T_b}{T}\right)\right] + \sigma\kappa\right]\mathbf{n} + \gamma[\boldsymbol{\nabla} T - \mathbf{n}(\boldsymbol{\nabla} T \cdot \mathbf{n})], \tag{3}$$

$$\frac{\partial F}{\partial t} + (\mathbf{u} \cdot \boldsymbol{\nabla}) F = 0, \tag{4}$$

$$\rho\left[\frac{\partial h}{\partial t} + (\mathbf{u} \cdot \boldsymbol{\nabla}) h\right] = \boldsymbol{\nabla} \cdot (k \boldsymbol{\nabla} T) + Q'''_{interface}, \tag{5}$$

$$h = h_{ref} + c_{p,bulk}\left(T - T_{ref}\right) + f_l \Delta H_{sl}. \tag{6}$$

The third term on the right hand side of equation (2) is related to the solidification drag forces and the rest of the interface-related volumetric forces, namely the recoil pressure, capillarity and the Marangoni effect are expressed in equation (3). The free surface of the fluid is tracked via the VOF method. The energy balance is expressed in equation (5) where ρ (kg.m^{-3}), k (W.m^{-1}.K^{-1}) and h (J.kg^{-1})

are density, thermal conductivity and enthalpy of the metal, respectively. The enthalpy term in its full form including the latent heat of fusion ΔH_{sl} (J.kg^{-1}) is shown in equation (6) and f_l (-) is the liquid fraction function. Thermal boundary conditions such as convection, radiation, evaporation and the laser heating are transformed into volumetric heat sources, involved in the Q''' (W.m^{-3}) term in equation (5), and then imposed within the boundary cells that are neighboring the void domain.

The computational domain of the model is shown in Figure 1 and the overall dimensions of the control volume are accordingly 2000 µm by 200 µm by 550 µm along x, y and z, respectively. A symmetric boundary condition is set at the x=0 plane where the laser passes and according to Figure 1, the upper and lower part of the domain are meshed with two different cell sizes of 6 µm and 20 µm, respectively. The fine mesh region is set to capture detailed fluid dynamics within the melt pool while the course-mesh region is supposed to model the thermal effect of the already manufactured layers. Furthermore, the current mesh configuration is found based on the mesh independency analysis carried out in the recent previous work of the authors [12].

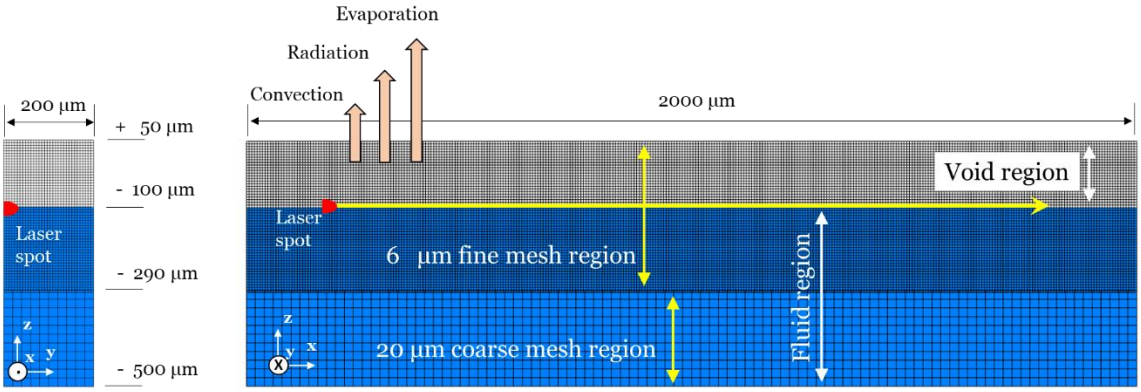

Figure 1: Front and side views of the computational domain. Note that the region along z and from -100 µm to +50 µm is void.

The thermal boundary conditions including convection, radiation and evaporation as well as the interface-related fluid dynamics forces are imposed on the free surface of the fluid domain.

In this work as mentioned earlier in the manuscript, a CFD model of the modulated PL-PBF process is developed. In the modulated PL-PBF process, the laser is only on over a fraction of a cycle period Δt_{cycle} (s) and this fraction is called duty cycle F (-) and it is expressed by percentage. The rest of the input process parameters in this study are 250 W power, 210 mm.s^{-1} scan speed and 100 µm beam size.

3. RESULTS AND DISCUSSIONS

In this work, a parametric study is carried out to investigate the impact of the cycle period on the melt pool behavior. Therefore, the cycle period Δt_{cycle} (s) is set to 400 µs, 1000 µs and finally, 3000 µs. The duty cycle F (-) is set to 50 % and finally 100 %, which leads to the continuous wave (CW) laser mode. The calculated temperature contours as well as the velocity field vector for the three different cycle periods for the 50 % duty cycle are shown at different times in Figure 2.

According to Figure 2 (a) – (c), humps forming at the wake of the melt pool for the Δt_{cycle} = 400 µs are very congested and dense and with noticeable overlap. These humps are results of the liquid metal re-deposition at the wake of the melt pool and then its following rapid solidification. It is in essence the recoil pressure that pumps the liquid metal backwards (due to liquid metal's incompressibility) and causes the re-deposition.

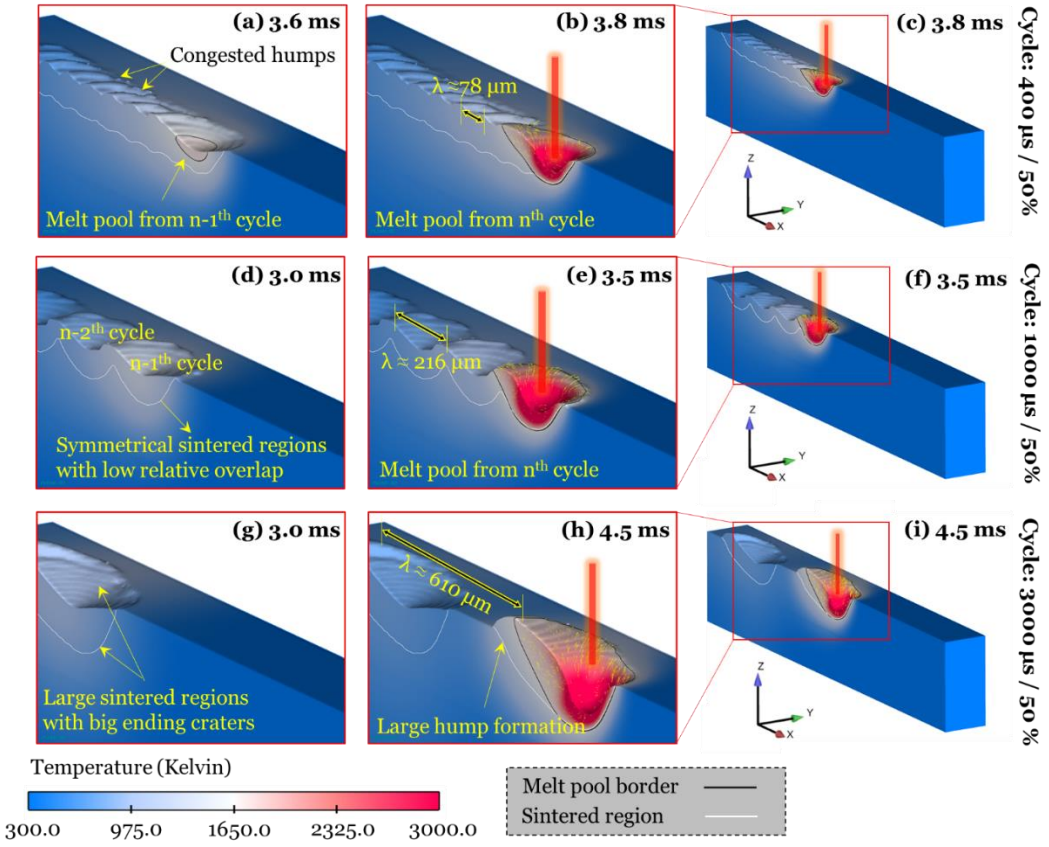

Figure 2: Temperature contours and melt pool border lines at different times for the 50 % duty cycle case: (a) - (c) Δt_{cycle} = 400 µs, (d) – (f) Δt_{cycle} = 1000 µs and (g) – (i) Δt_{cycle} = 3000 µs.

According to Figure 2 (b), the distance between two neighboring humps is about 78 µm and this is roughly the distance, which the laser with 210 mm.s^{-1} speed passes over a 400 µs cycle. Based on Figure 2 (d) – (f) and Table 1, by raising the cycle period to 1000 µs, the melt pool becomes more symmetrical and at the same time deeper, compared to the 400 µs case.

Table 1: Melt pool dimensions and track shape at 50 % duty cycle.

Δt_{cycle} (s)	Hump (µm)	Crater (µm)	Depth (µm)	Length (µm)
400 µs	12	6	64	279
1000 µs	16	23	78	240
3000 µs	41	40	145	374

On the other side, the melt pool is longer in the 400 µs case compared to the 1000 µs case and the main reason behind this is the fact that the laser off-time period for the former case is 200 µs compared to the 500 µs for the latter case and which is 2.5 times longer. In this situation and for shorter cycle periods, the laser off-time will be shorter and therefore there will be more significant pre-heating for the newly-formed melt pools. According to Figure 2 (a), at 3.6 ms, and at the end of the n-1th cycle, there is a small amount of liquid metal still left and then this remaining melt pool region merges with the new melt pool formed at the nth cycle and therefore the overall melt pool length will be longer for the 400 µs case. It is also interesting to notice that the hump size increases with the increase in the cycle period and that is because for longer cycle periods, more material re-deposition occurs that in turn leads to bigger hump formations. Furthermore, according to data given in Table 1, the crater size also increases with the increase in the cycle period. This is primarily due to the fact that more material will be re-deposited

at longer cycle periods and since there is no material input to the cases studied above, bigger craters form at the end of the tracks because of mass conservation. According to Table 1, the crater size increases from 6 μm at 400 μs cycle period to 40 μm at 3000 μs cycle period.

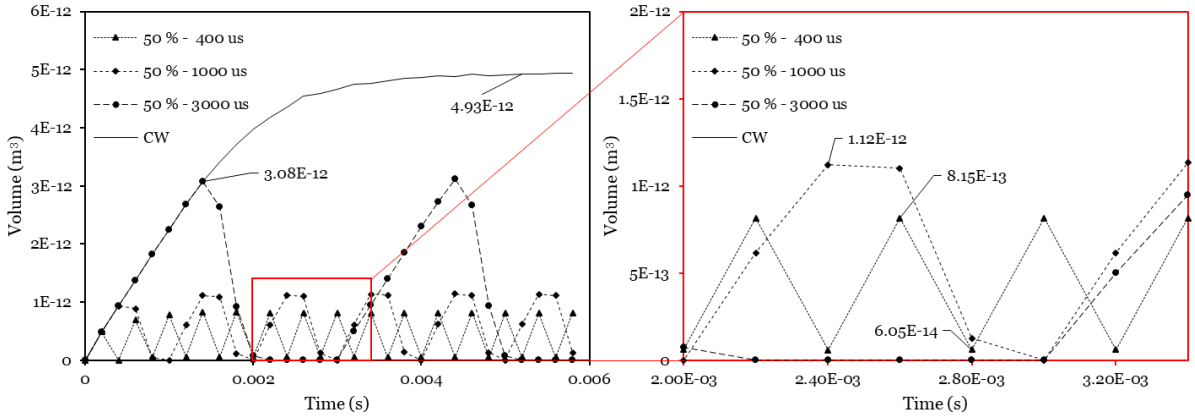

Figure 3: Plot of melt pool volume versus time for four cases including continuous wave laser as well as 50 % duty cycle at 400 μs, 1000 μs and 3000 μs.

The plot of melt pool volume against time is shown in Figure 3 for the continuous wave laser and the three cases at 50 % duty cycle. One can clearly see that the melt pool's volume for all the three cases of 50 % duty cycle, follow the trend of the melt pool volume at the continuous wave mode. Moreover, the maximum melt pool volume increases with the elongation of cycle period, since as expected, the laser-material's contact time becomes longer, thus more energy is absorbed within each cycle, leading to larger melt pools eventually. Furthermore, it is noticed in the blow-up part of Figure 3 that, as opposed to the 1000 μs and 3000 μs cases, in the 400 μs case, the melt pool volume never becomes zero over the laser's off-time period and those small remnants of liquid metal from previous cycles merge with the newly formed melt pools and this leads to longer melt pools in the end.

4. CONCLUSIONS

In this work a CFD model of the modulated PL-PBF process of stainless steel 316-L is developed in the commercial software package Flow-3D. The model involves physics such as solidification, melting, evaporation, convection, laser-material interaction, capillarity, Marangoni effect and the recoil pressure effect. In the current study, a parametric study is carried out to understand how the change in the cycle period duration affects the melt pool's thermo-fluid conditions during the modulated PL-PBF process. It is observed that at the pulse mode with 50 % duty cycle and 400 μs cycle period, an overlapped chain of humps form at the wake of the melt pool and at a spatial frequency of occurrence of about 78 μm. Furthermore and as expected, it is noted that the melt pool volume, the size of the hump as well as the crater size at the end of the track, increase with increase in the cycle period duration, as more material is re-deposited at the back of the melt pool and that itself is caused by more pronounced recoil pressures. Moreover, it is noticed that due to the short off-time period of the laser in the 400 μs cycle period case, there is always an amount of liquid metal left from the previous cycle, at the time the new cycle starts. This is found to be the main reason why longer and elongated melt pools form at 400 μs cycle period, compared to the bigger, shorter and more symmetrical-like melt pools forming at the 1000 μs case. In this study PL-PBF single tracks including the broken track and the continuous track examples were studied to illustrate the boundary of this transition at a given laser scan parameter setting. At higher scan speeds, it is expected that the Plateau–Rayleigh instability will compete with the pulsing behavior to change the transition boundary between a broken and continuous track, which is suggested as future work from this study.

ACKNOWLEDGEMENTS

This work has received funding from Independent Research Fund Denmark, DIGI-3D project [0136-0210B].

REFERENCES

[1] T. Craeghs, L. Thijs, F. Verhaeghe, J.-P. Kruth, J. Van Humbeeck, A study of the microstructural evolution during selective laser melting of Ti–6Al–4V, Acta Mater. 58 (2010) 3303–3312. https://doi.org/10.1016/j.actamat.2010.02.004.

[2] J. Liu, A.T. Gaynor, S. Chen, Z. Kang, K. Suresh, A. Takezawa, L. Li, J. Kato, J. Tang, C.C.L. Wang, L. Cheng, X. Liang, A.C. To, Current and future trends in topology optimization for additive manufacturing, (2018) 2457–2483.

[3] M. Bayat, W. Dong, J. Thorborg, A.C. To, J.H. Hattel, A review of multi-scale and multi-physics simulations of metal additive manufacturing processes with focus on modeling strategies, Addit. Manuf. 47 (2021). https://doi.org/10.1016/j.addma.2021.102278.

[4] A. Foroozmehr, M. Badrossamay, E. Foroozmehr, S. Golabi, Finite Element Simulation of Selective Laser Melting process considering Optical Penetration Depth of laser in powder bed, Mater. Des. 89 (2016) 255–263. https://doi.org/10.1016/j.matdes.2015.10.002.

[5] Y.S. Lee, W. Zhang, Modeling of heat transfer, fluid flow and solidification microstructure of nickel-base superalloy fabricated by laser powder bed fusion, Addit. Manuf. 12 (2016) 178–188. https://doi.org/10.1016/j.addma.2016.05.003.

[6] S.A. Khairallah, A.T. Anderson, A. Rubenchik, W.E. King, Laser powder-bed fusion additive manufacturing: Physics of complex melt flow and formation mechanisms of pores, spatter, and denudation zones, Acta Mater. 108 (2016) 36–45. https://doi.org/10.1016/j.actamat.2016.02.014.

[7] M. Bayat, A. Thanki, S. Mohanty, A. Witvrouw, S. Yang, J. Thorborg, N.S. Tiedje, J.H. Hattel, Keyhole-induced porosities in Laser-based Powder Bed Fusion (L-PBF) of Ti6Al4V: High-fidelity modelling and experimental validation, Addit. Manuf. 30 (2019). https://doi.org/10.1016/j.addma.2019.100835.

[8] A. Charles, M. Bayat, A. Elkaseer, L. Thijs, J.H. Hattel, S. Scholz, Elucidation of dross formation in laser powder bed fusion at down-facing surfaces: phenomenon-oriented multiphysics simulation and experimental validation, Addit. Manuf. Under revi (2021).

[9] M. Bayat, V.K. Nadimpalli, D.B. Pedersen, J.H. Hattel, A fundamental investigation of thermo-capillarity in laser powder bed fusion of metals and alloys, Int. J. Heat Mass Transf. 166 (2021) 120766. https://doi.org/10.1016/j.ijheatmasstransfer.2020.120766.

[10] J.D. Roehling, S.A. Khairallah, Y. Shen, A. Bayramian, C.D. Boley, A.M. Rubenchik, J. Demuth, N. Duanmu, M.J. Matthews, Physics of large-area pulsed laser powder bed fusion, Addit. Manuf. 46 (2021) 102186. https://doi.org/10.1016/j.addma.2021.102186.

[11] M. Zheng, L. Wei, J. Chen, Q. Zhang, J. Li, S. Sui, G. Wang, W. Huang, Surface morphology evolution during pulsed selective laser melting: Numerical and experimental investigations, Appl. Surf. Sci. 496 (2019) 143649. https://doi.org/10.1016/j.apsusc.2019.143649.

[12] M. Bayat, V.K. Nadimpalli, D.B. Pedersen, J.H. Hattel, A fundamental investigation of thermo-capillarity in laser powder bed fusion of metals and alloys, Int. J. Heat Mass Transf. 166 (2021). https://doi.org/10.1016/j.ijheatmasstransfer.2020.120766.